Research Article

ADVANCED PHOTONICS

Nonlinear topological valley Hall edge states arising from type-II Dirac cones

Hua Zhong,[a,†] Shiqi Xia,[b,†] Yiqi Zhang,[a,*] Yongdong Li,[a] Daohong Song,[b,*] Chunliang Liu,[a] and Zhigang Chen[b,c,*]

[a]Xi'an Jiaotong University, School of Electronic Science and Engineering, Key Laboratory for Physical Electronics and Devices of the Ministry of Education & Shaanxi Key Lab of Information Photonic Technique, Faculty of Electronic and Information Engineering, Xi'an, China

[b]Nankai University, TEDA Applied Physics Institute and School of Physics, MOE Key Laboratory of Weak-Light Nonlinear Photonics, Tianjin, China

[c]San Francisco State University, Department of Physics and Astronomy, San Francisco, California, USA

Abstract. A Dirac point is a linear band crossing point originally used to describe unusual transport properties of materials like graphene. In recent years, there has been a surge of exploration of type-II Dirac/Weyl points using various engineered platforms including photonic crystals, waveguide arrays, metasurfaces, magnetized plasma and polariton micropillars, aiming toward relativistic quantum emulation and understanding of exotic topological phenomena. Such endeavors, however, have focused mainly on linear topological states in real or synthetic Dirac/Weyl materials. We propose and demonstrate nonlinear valley Hall edge (VHE) states in laser-written anisotropic photonic lattices hosting innately the type-II Dirac points. These self-trapped VHE states, manifested as topological gap quasi-solitons that can move along a domain wall unidirectionally without changing their profiles, are independent of external magnetic fields or complex longitudinal modulations, and thus are superior in comparison with previously reported topological edge solitons. Our finding may provide a route for understanding nonlinear phenomena in systems with type-II Dirac points that violate the Lorentz invariance and may bring about possibilities for subsequent technological development in light field manipulation and photonic devices.

Keywords: photonic topological insulator; type-II Dirac cone; valley Hall edge soliton.

Received Jul. 31, 2021; revised manuscript received Sep. 12, 2021; accepted for publication Sep. 29, 2021; published online Oct. 22, 2021.

[DOI: 10.1117/1.AP.3.5.056001]

1 Introduction

Loosely speaking, topological insulators in condensed matter physics refer to materials that only allow electrons to conduct along the surface but not in bulk.[1,2] The concept was introduced into the realm of photonics about a dozen years ago, and has since led to the burgeoning development in photonic topological insulators (PTIs)[3–13] and topological photonics in general.[14,15]

Recently, nonlinear topological photonics has attracted increasing attention,[16] as nonlinearity exists inherently in many photonic topological systems such as topological insulator lasers[17–21] and nonlinearity-induced topological insulators.[22,23] Topological solitons, for example, have been proposed in several photonic settings,[24–31] which typically require breaking of the time-reversal-symmetry (TRS) by applying external magnetic fields or equivalently the z-reversal symmetry by nontrivial longitudinal modulation. Indeed, topological bandgap solitons were recently observed in the bulk of an anomalous PTI,[32] which relied on a Kerr nonlinearity and periodic driving of anomalously coupled waveguide arrays.[33,34]

It is natural to ask if topological edge solitons can exist in a TRS-preserved system, or systems without complex modulation or external magnetic fields, which is essential for practical applications. For instance, coupling and locking of semiconductor laser arrays to produce coherent high-power laser sources is one of the key motivations behind the development of topological insulator lasers.[17–21] The most promising approach could rely on PTI symmetry design,[35] such as using the valley Hall effect[36–39] without breaking the TRS. Relevant progress on photonic valley

*Address all correspondence to Yiqi Zhang, zhangyiqi@xjtu.edu.cn; Daohong Song, songdaohong@nankai.edu.cn; Zhigang Chen, zhigang@sfsu.edu

†The authors contributed equally to this work.

Hall effect can be found in a recent review.[40] Indeed, it has been demonstrated that valley Hall edge (VHE) states can be used in topological laser fabrication[41] and on-chip communications.[42,43] Even though gap solitons were found in the Dirac model,[44] VHE solitons have never been realized as they are completely different from all previously investigated solitons: the topological VHE soliton is an inheritor of the linear VHE state, so its appearance does not feature power threshold, in sharp contrast to those standard photonic bandgap solitons.[45–52]

A general consensus is that many topological and valley Hall effects are mediated by materials with nontrivial degeneracy in momentum space, characterized by Dirac/Weyl cones. In the two-dimensional case, a well-celebrated example is graphene, in which electrons around the Dirac cones behave as massless Dirac fermions. Different from type-I Dirac cones in graphene where the corresponding Fermi surface is a point, there are also so-called tilted type-II Dirac cones with the Fermi surface being a pair of crossing lines.[53–64] Type-II Dirac cones violate the Lorentz symmetry, thus allowing for quasi-particle-mediated phenomena that do not exist in high-energy physics analogically investigated in condensed matter physics. In photonics, for example, type-II Dirac cones are expected to bring new features due to their nonisotropic transport properties arising from the distinctive dispersions. Photonic lattices can be readily designed to possess such Dirac cones,[54,57] making them attractive for investigation of nontrivial topological phenomena.[61]

In this work, as one typical example, we propose and demonstrate experimentally a scheme to establish type-II Dirac photonic lattices in a nonlinear medium and, more importantly, to reveal the existence of topologically protected nonlinear VHE states. Such nonlinear VHE states in Dirac systems have inherited topological features from their linear counterparts,[65] thus benefiting from easy implementation without any need of "time" modulation or external magnetic fields.

2 Principles and Methods

The propagation of a light beam in a photonic lattice is described by the Schrödinger-like paraxial wave equation:

$$i\frac{\partial\psi(\xi,\eta,\zeta)}{\partial\zeta}=-\frac{1}{2k_0}\left(\frac{\partial^2}{\partial\xi^2}+\frac{\partial^2}{\partial\eta^2}\right)\psi(\xi,\eta,\zeta)-\frac{k_0\Delta n(\xi,\eta)}{n_0}\psi(\xi,\eta,\zeta),\tag{1}$$

where $k_0=2n_0\pi/\lambda_0$ is the wave number in the crystal with refractive index n_0. Note that ζ in Eq. (1) plays the role of time in the quantum mechanics Schrödinger equation.[5] For the specific photorefractive strontium barium niobite (SBN) crystal used in our experiment, we take

$$\Delta n(\xi,\eta)=-\frac{1}{2}n_0^3\gamma_{33}E_0\frac{1}{1+I(\xi,\eta)},\tag{2}$$

with $I(\xi,\eta)$ being the intensity pattern of the lattice beam that is measured in units of the background illumination.[66] The parameters corresponding to experiment are $\lambda_0=532$ nm, $n_0=2.35$, the bias field $E_0=1$ kV/cm, and the electro-optic coefficient $\gamma_{33}=280$ pm/V.[47,51] The refractive index change reaches typically $\Delta n\sim1.82\times10^{-4}$. In experiment the lattices are written point by point; the corresponding lattice intensity pattern can be considered as an appropriate superposition of Gaussian beams $I(\xi,\eta)=|\sum_{l=\{A,B,C\},m}\delta_l\exp\{-[(\xi-\xi_m)^2+(\eta-\eta_m)^2]/w^2\}|^2$ in which δ_l represents the beam amplitude, (ξ_m,η_m) is the beam center, A,B,C represent the lattice sites, and m is an integer. The distance between two nearest-neighbor sites is set to be $d=30$ μm and $w=0.32d$. The diffraction length is $L_\zeta=k_0\rho_0^2$, with $\rho_0=12$ μm representing the typical width of the experimental incident beam. If we replace ξ,η,ζ by $\rho_0x,\rho_0y,L_\zeta z$, one obtains the dimensionless version of Eq. (1), which is

$$i\frac{\partial\psi(x,y,z)}{\partial z}=-\frac{1}{2}\left(\frac{\partial^2}{\partial x^2}+\frac{\partial^2}{\partial y^2}\right)\psi(x,y,z)-\frac{k_0^2r_0^2\Delta n(x,y)}{n_0}\psi(x,y,z),\tag{3}$$

the solution of which can be written as $\psi(x,y,z)=u(x,y)\exp(-i\beta z)$ with β being the propagation constant and $u(x,y)$ being the Bloch function. We would like to note that there is a minus sign in the solution, so that the sign of β is completely opposite if the solution without the minus sign is adopted. When nonlinearity is considered, the refractive index change is written as

$$\Delta n(x,y,z)=-\frac{1}{2}n_0^3\gamma_{33}E_0\frac{1}{1+I(x,y)+|\psi(x,y,z)|^2},\tag{4}$$

which is dependent on the beam intensity $|\psi(x,y,z)|^2$ upon propagation. With the nonlinear refractive index change, the solution can be written as $\psi(x,y,z)=u(x,y)\exp(-i\mu z)$ with μ being the nonlinear propagation constant.

An exemplary type-II Dirac photonic lattice is displayed in Fig. 1(a) with $\delta_l=4$, and its Brillouin zone (BZ) spectrum is shown in Fig. 1(b) in which the first BZ is indicated by the shaded hexagon. The design process of type-II Dirac photonic lattices can be found in the Supplementary Material. There are three sites in each unit cell of the type-II lattice, and they are labeled as A, B, and C in Fig. 1(a). Such a lattice can be considered as the direct outcome from properly stretching a dislocated Lieb lattice in the vertical direction.[67] The experimental lattice structure and measured BZ spectrum shown in Figs. 1(c) and 1(d) match perfectly with the numerical results in Figs. 1(a) and 1(b). Moreover, we calculate the band structure of the type-II lattice as shown in Fig. 1(e) based on the plane-wave expansion method. Evidently, under proper lattice design, the bands are tilted and connected at some points—the type-II Dirac points, which are induced solely by the spatial geometry of the lattice.[67] To see more clearly, we zoom in on one Dirac cone indicated by a red circle in Fig. 1(e), and let one horizontal plane (corresponding to the Fermi surface) go across the Dirac point. The intersection at the Dirac cone forms a pair of crossing lines in the momentum space [see the inset in Fig. 1(f)]—the characteristic feature of the type-II Dirac cone.[61]

3 Results

3.1 Linear Valley Hall Edge States

In Fig. 1(a), the lattice is uniform, but if we intentionally introduce a detuning to one site in the unit cell, the inversion

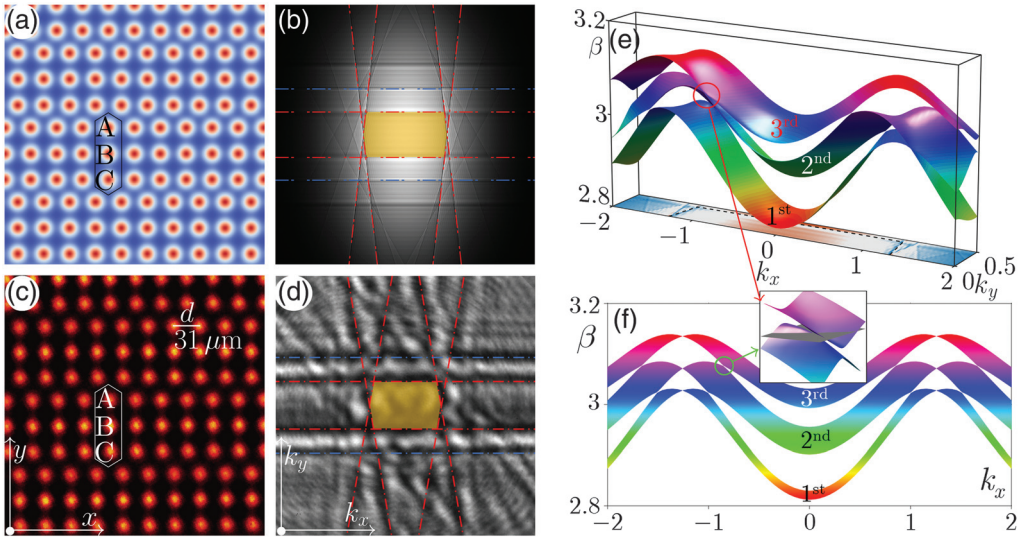

Fig. 1 Photonic lattices with type-II Dirac cones. (a) Numerically designed lattice structure with *A*, *B*, and *C* marked as the three sites in a unit cell indicated by a hexagon. Red spots represent the lattice sites. (b) BZ spectrum of (a) with the red dashed lines contouring the first BZ (shaded region). (c), (d) Experimental realization of the lattice and its BZ spectrum measured with the white-light BZ spectroscopy technique, corresponding to (a) and (b). In panel (c), bright spots represent the lattice sites. (e) Band structure of the photonic lattice in which type-II Dirac points exist due to the tilted band-touching between the first and second bands, and second and third bands. The projected BZ is shown in the (k_x, k_y) plane. (f) Projection of the band structure in the (k_x, β) plane. The inset is a zoom-in plot of the type-II Dirac cone indicated by circles with arrows. The gray horizontal plane in (k_x, k_y) coordinates goes across the Dirac point and intersects with the Dirac cone to form a pair of crossing lines—a direct manifestation of the type-II Dirac cone.

symmetry of the lattice will be broken. In Fig. 2(a), we intentionally increase the depth of site C from $\delta_C = 4$ to $\delta_C = 4.5$, and in Fig. 2(b), we increase the depth of site A from $\delta_A = 4$ to $\delta_A = 4.5$, while keeping that of other sites still at $\delta_l = 4$. The band crossings in the band structure indeed disappear as the gap opens, as shown in Fig. 2(c). We also display the calculated Berry curvature Ω of the first band in the (k_x, k_y) plane shown in Fig. 2(d), with the red and blue colors representing the positive and negative values. The valley Chern number $C_v = \frac{1}{2\pi}\iint_{\text{valley}} \Omega(k_x, k_y) \mathrm{d}k_x\, \mathrm{d}k_y$ can be numerically obtained for each valley, which is $C_v = \pm 1/2$. One finds that the Berry curvatures of the first band corresponding to Figs. 2(a) and 2(b) are opposite. Therefore, a domain wall (DW) can be established between two lattices with different index detunings, as shown in Fig. 2(e), where the DW is outlined by a rectangle. Crossing the DW in the y direction, the difference of the valley Chern numbers is $|\Delta C_v| = |\pm 1/2 - (\mp 1/2)| = 1$, which indicates that a topologically nontrivial edge state emerges along the DW. Note that the lattice in Fig. 2(e) is periodic along the x direction. The corresponding band structure $\beta(k_x)$ is displayed in Fig. 2(f). The black curves in the band structure represent the bulk states, whereas the red curve in the bandgap is the VHE state that distributes along the DW. We would like to note that the edge state may also appear in the bandgap between the second and third bulk bands if different inversion symmetries are applied, as discussed in detail in the Supplementary Material.

3.2 Nonlinear Valley Hall Edge States and Quasi-Solitons

The appearance of topological edge solitons inherited from their linear counterparts strongly depends on the dispersion condition of the linear topological edge states.[27] One may obtain bright solitons or dark solitons depending on the different dispersions for given self-focusing nonlinearity. Indeed, the inversion-symmetry-breaking perturbation lifts the degeneracy at Dirac points. However, the bands do not lose their symmetry properties around the Dirac points and affect the dispersions of the VHE states. According to our numerical analysis, the VHE states arising from type-II Dirac cones fulfill the dispersion condition ($\beta'' > 0$, i.e., the normal dispersive regime), which is a necessary condition for the existence of bright VHE solitons, but such a condition is not satisfied for the type-I Dirac photonic lattices. However, we do not claim that VHE solitons are not supported in lattices with type-I Dirac cones. In fact, the realization of VHE solitons from type-I Dirac cones is still an open question and merits further exploration. We thus solve for the first-order derivative β' (group velocity of the edge state) and the second-order derivative β'' of the linear VHE state in Fig. 2(f), and the results are displayed in Fig. 3(a). Here the VHE state with $\beta' > 0$ moves along the positive x direction. Notedly, as shown in Fig. 3(a), the normal dispersion ($\beta'' > 0$) region is $-0.235 \leq k_x/K \leq 0.235$, where $K = 2\pi/d$ defines the width of the first BZ. By adopting the Newton method, we found a

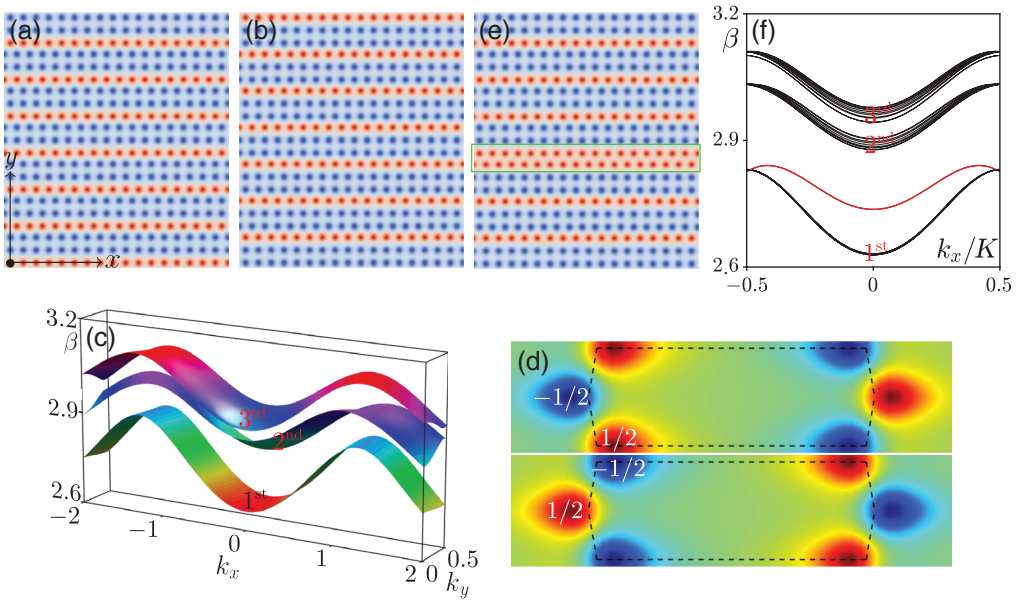

Fig. 2 Linear topological VHE states at the DW between two type-II Dirac cone photonic lattices. (a) and (b) Inversion-symmetry-broken photonic lattices with the depth of site *C* and site *A* increased, respectively. (c) Band structure corresponding to the lattice in (a) [which looks the same for the lattice in (b)]. (d) Berry curvature of the first band displayed in the (k_x, k_y) plane. The top panel corresponds to (a); the bottom panel, which is opposite, corresponds to (b). The dashed hexagon represents the first BZ. (e) A DW is established by combining (a) and (b) with an interface, highlighted by a green rectangle. The lattice is periodic along the *x* direction but has boundaries along the *y* direction. (f) Band structure of the lattice in (e); the red curve represents the topologically protected VHE state along the DW. In panels (a), (b), and (e), blue and red spots represent the lattice sites with different detunings.

family of such nonlinear solutions: the peak amplitude $a = \max\{|\psi|\}$ and power $P = \iint |\psi|^2 \mathrm{d}x\,\mathrm{d}y$ of the nonlinear VHE states at $k_x/K = 0.1$ are plotted in Fig. 3(b) as a function of the nonlinearity-dependent propagation constant μ. One finds that both $a(\mu)$ and $P(\mu)$ decrease as μ increases, reducing to nearly zero at $\mu \sim 2.741$ where the nonlinear localized states resemble or reduce to the linear ones.

Let us now examine the modulational instability (MI) of nonlinear VHE states under the action of self-focusing nonlinearity, which is possible since $\beta'' > 0$ at $k_x/K = 0.1$. To do so, we add a random noise to the nonlinear VHE state obtained at $\mu = 2.736$, with a noise amplitude about 5% of the nonlinear edge state shown in Fig. 3(c). Representative propagation of the peak amplitude $a = \max\{|\psi|\}$ of the perturbed state is shown in Fig. 3(d). The amplitude profiles of the nonlinear edge state at two selected distances [marked by two red dots in Fig. 3(d)] are displayed in Fig. 3(c), showing growth of MI during propagation which leads to formation of quasi-soliton filaments along the DW. The larger the noise amplitude is (e.g., 10% of the nonlinear edge state), the faster the growth of the MI is, and the quicker the formation of quasi-soliton filaments. These MI-induced soliton filaments are considered as precursors for the formation of optical solitons,[26] but here they also benefit from the topological protection inherited from the corresponding linear VHE states. Without loss of generality, we take out one of such bright filaments at $z = 1750$ [indicated by a red circle in Fig. 3(c)] as the input and investigate its long-distance propagation dynamics. To this end, we introduce another physical quantity—the barycenter of the filament defined as $x_c = P^{-1} \iint x|\psi|^2 \mathrm{d}x\,\mathrm{d}y$—to record its movement during propagation. We first shift the selected filament in Fig. 3(c) to the center of the window ($x = 0$) and then track its propagation. The peak amplitude and barycenter of the filament are displayed in Fig. 3(e), showing the stability of a moving VHE quasi-soliton. Even over an extremely long propagation distance ($z \sim 32{,}000$), the peak amplitude remains nearly invariant and the barycenter exhibits a saw-tooth-like oscillating behavior. The appearance of the saw-tooth behavior in the center of mass of the wavepacket is mainly due to the simulation method (the split-step Fourier method) we adopted: for a chosen window along x, part of the transporting VHE quasi-soliton appears at the left end of the numerical window when it reaches the right end, resulting in an apparent periodic jump of the barycenter between two ends. The same reason holds for the panel with $z = 1000$ in Fig. 3(g). In Fig. 3(f), snapshots of the quasi-soliton taken at different propagation distances are displayed. We observe clearly that the quasi-soliton moves along the positive x direction with a constant speed (it is same as β'), and it remains localized with negligible radiation loss either along the DW or into the bulk—a result of interplay between nonlinearity and topological protection. For direct comparison, we propagate the same input filament in the linear lattice, i.e., removing the nonlinear term $|\psi(x, y, z)|^2$ in Eq. (4). As expected, without the balance from the nonlinearity, the filament spreads quickly along the DW because of diffraction [see Fig. 3(g)], yet remains localized in the direction perpendicular to the DW. Here we only discuss the case of VHE solitons with $\mu = 2.736$, but the approach and analysis also apply to other parameter cases.

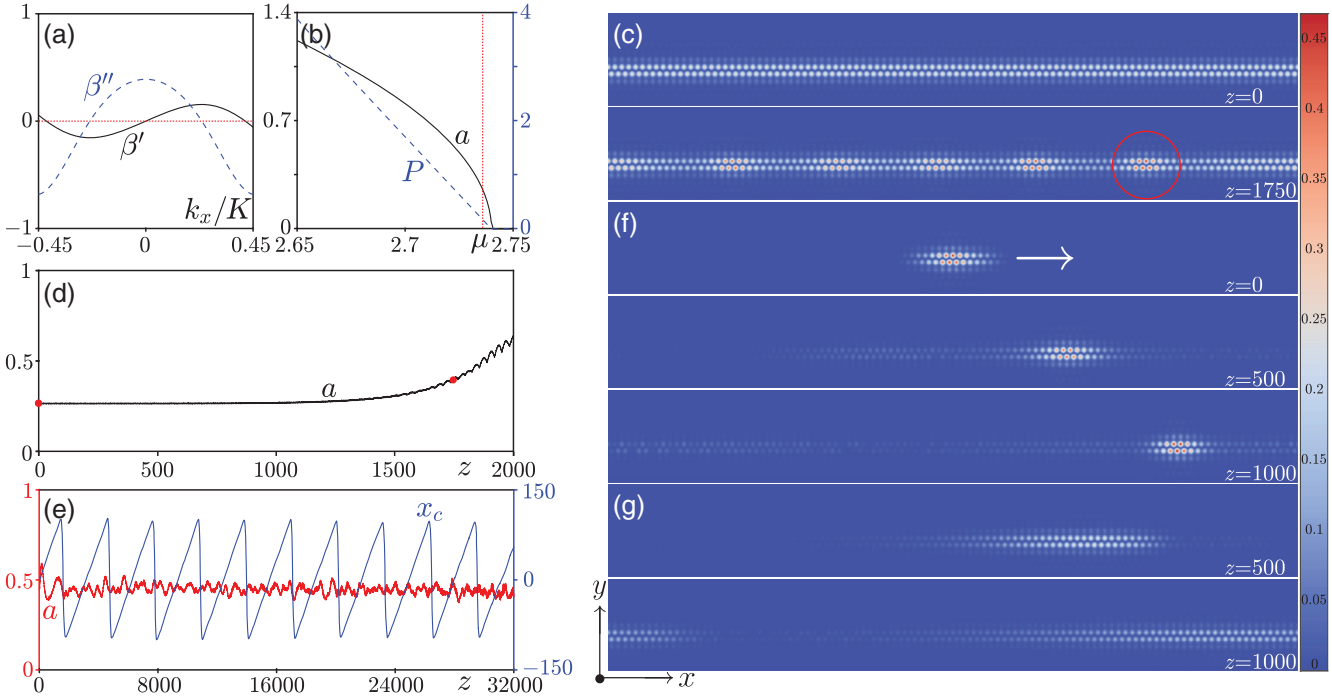

Fig. 3 Numerically obtained nonlinear topological VHE states and robust transport of quasi-solitons from MI. (a) Dispersion spectrum of the linear edge state in Fig. 2(f). Solid curve is for β' and dashed curve for β''. VHE quasi-solitons are found only in the region with $\beta'' > 0$. (b) Plots of amplitude a and power P of the nonlinear edge states at $k_x = 0.1K$ versus μ. The red dotted line corresponds to $\mu = 2.736$. (c) Profiles of a typical nonlinear edge state (superimposed with 5% random noise) found at $\mu = 2.736$ at $z = 0$ and $z = 1750$. (d) Amplitude of the nonlinear state in (c) versus propagation distance. (e) Amplitude a (red curve) and barycenter x_c (blue curve) of a quasi-soliton filament [marked by the red circle in (c)] resulting from MI, showing the robustness of the quasi-soliton over extremely long distances, as seen also in the intensity pattern snapshots (f) during transport. (g) Spreading of the same input at $z = 0$ as in (f) along the DW during linear propagation for comparison. (Here, $z = 1000$ corresponds to a physical distance 4 m.)

Since there is no power threshold for the nonlinear VHE state [see the continuous peak amplitude and power curves in Fig. 3(b)], the corresponding quasi-soliton possesses a higher intensity if it bifurcates from the nonlinear VHE state with a larger amplitude. Since the nonlinearity can induce a defect in the topological structure, the topological property will be broken if the strength of the defect is larger than the bandgap width. From this point of view, one cannot seek for the VHE solitons with very high intensity. In the region with $\mu > 2.736$, the obtained solitons have a smaller peak amplitude and intensity. It is impossible to design corners for the DW of type-II Dirac photonic lattices due to the spatial symmetry, yet artificial corners can play a role of disorder but would result in intervalley scattering due to weak valley protection. Such issues are further addressed in the Supplementary Material, where we use a large-scale random disorder to check the robustness of the VHE solitons.[68–70]

3.3 Experimental Observation of Nonlinear Valley Hall Edge States

In the experiment, an inversion-symmetry-broken type-II Dirac photonic lattice with a DW [corresponding to Fig. 2(e)], as shown in Fig. 4(a1), is established by employing the CW-laser-writing technique (similar for writing the uniform lattice in Fig. 1(c) but with a judiciously controlled writing process).[71–73] The technique relies on writing the waveguides site-by-site in a 10-mm-long nonlinear photorefractive crystal (SBN:61 with cerium doping: 0.002% CeO_2). The experimental setup (more details about the setup can be found in the Supplementary Material) involves a continuous wave laser beam ($\lambda = 532$ nm) to illuminate a spatial light modulator, which creates a quasi-non-diffracting writing beam with variable input positions. Because of the noninstantaneous photorefractive "memory" effect, all waveguides remain intact during the writing and the subsequent probing processes. After the writing process, the lattice structure can be examined by sending a broad beam (quasi-plane-wave) to visualize the whole lattice. Once the structure is established, the probe beam is used to excite the lattice along the DW, and it can undergo either linear propagation (when the bias field is turned off) or experience a self-focusing nonlinearity under a positive bias field. Of course, the probe beam can locally change the index structure of the lattices due to its self-action during nonlinear propagation—the ingredient needed to study the nonlinear effects experimentally.[72,73]

To appreciate the formation of nonlinear VHE states presented in Fig. 3(e), two out-of-phase elliptical Gaussian beams (due to the property of the VHE state that has a staggered phase structure along the y axis) are superimposed as a probe beam with an input power of only 3 μW, whose position is marked by the white dashed oval in Fig. 4(a1). The linear and nonlinear

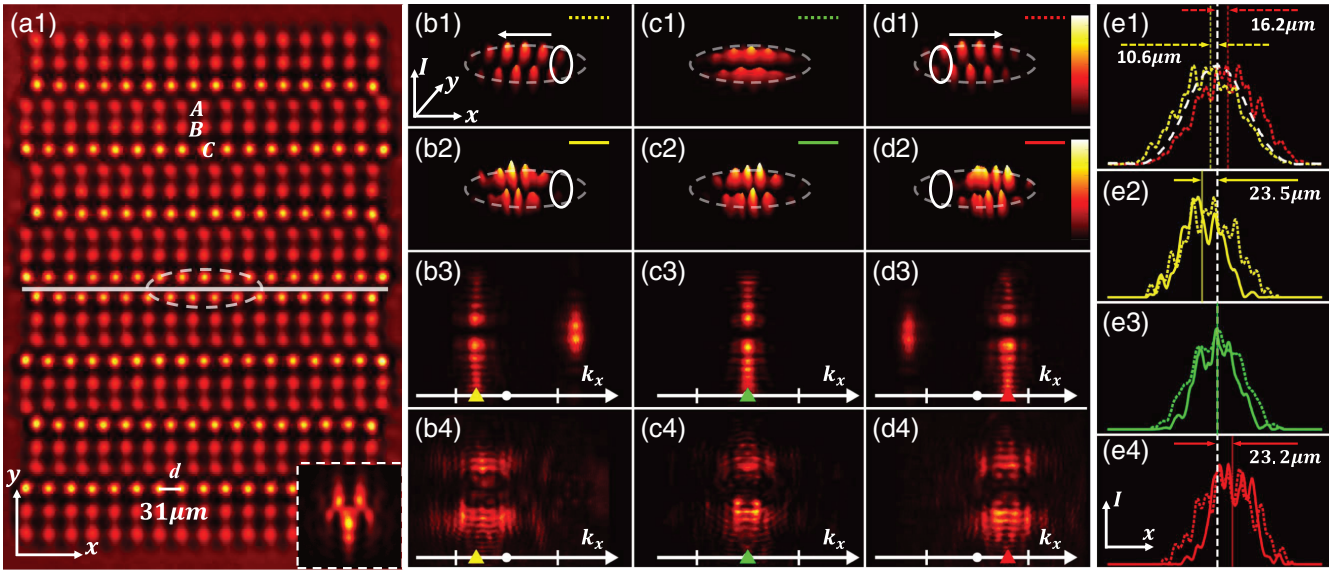

Fig. 4 Experimental observation of nonlinear topological VHE states. (a1) Experimentally established type-II Dirac lattices with a center DW (marked by the white line), where the inset (bottom-right) shows discrete diffraction from single-site excitation. (b)–(d) Linear (first and third rows) and nonlinear (second and fourth rows) outputs in real (first and second rows) and momentum (third and fourth rows) space obtained from excitation by two superimposed out-of-phase elliptical beams (circled by the dashed ellipse). The initial Bloch momenta of the probe beam are (b) $-3\pi/5d$, (c) 0, and (d) $3\pi/5d$, as marked by colored triangles in the spectra, where the white dots mark the BZ center for reference. The first two rows are presented under the same color scale as shown in (d1) and (d2). Solid ellipses in the top two rows mark the portion in the input beam that is "diminished" by nonlinearity. (e) Dashed (linear) and solid (nonlinear) curves illustrate the relative position of normalized intensity profiles of the output beam along the x axis, and vertical lines mark the corresponding center position of the beam. White dashed curve in (e1) corresponds to the input beam for reference. Shifting of the beam position in (b2) [e(2)] and (d2) [(e4)] signals the nonlinearity-induced transport of the VHEs, as analyzed in our theory and corroborated by numerical simulations.

output intensity patterns in real space and their corresponding spectra in momentum space for three different excitation conditions (e.g., with Bloch momentum $k_x/K = -0.3, 0, +0.3$) are shown in Figs. 4(b)–4(d). When the bias field is off, the probe beam itself does not exhibit nonlinear self-action, but it is localized in the vertical direction without spreading into the bulk due to the excitation of the linear VHE states, although somewhat extended along the DW after 1 cm of propagation. However, the probe beam undergoes self-focusing when the bias field is turned on (0.7 kV/cm) and, as a result, the corresponding nonlinear output also becomes more localized along the DW direction [Figs. 4(b2)–4(d2)]. This can be seen more clearly from the overall beam width [full width at half maximum (FWHM)], which decreased approximately from 100 μm (linear case) to 80 μm (nonlinear case) [Figs. 4(e2)–4(e4)]. Interestingly, we found that the output pattern moves slightly to the left (right) even in the linear condition for the Bloch momentum $k_x/K = -0.3\,(+0.3)$, thanks to the initial transverse velocity of the VHEs, while that for $k_x = 0$ remains invariant [Fig. 4(e1)]. Due to the nonlinear action, an appreciable portion (about 20%) is "diminished" from the initial position of the probe beam (marked by a solid ellipse) as compared with the linear case. This is a direct signature of nonlinearity-induced transport of the VHEs. Indeed, by using the barycenter of the beam defined earlier, and plotting the superimposed linear and nonlinear output profiles along the x direction [Figs. 4(e2)–4(e4)], we can see clearly that the center is further shifted away from the initial input position under nonlinear propagation. Furthermore, nonlinearity-induced spectral reshaping is evident due to formation of nonlinear VHEs by comparing nonlinear [Figs. 4(b4)–4(d4)] with linear [Figs. 4(b3)–4(d3)] output spectra. Our results indicate that self-trapped nonlinear VHE states indeed exist in type-II Dirac photonic lattices. Due to the limited crystal length, it is not feasible to experimentally show the long-distance transport of the quasi-solitons as demonstrated in our theoretical analysis. However, these experimental results in Fig. 4 are corroborated by numerical simulations, as detailed in the Supplementary Material. Here we would like to note that the waveguide is assumed uniform without appreciable losses along the propagation direction. Thus the transmission efficiency is nearly invariant for the probe beam.

4 Discussion and Conclusion

We have proposed and experimentally demonstrated photonic lattices exhibiting type-II Dirac points, thereby unveiling the existence of nonlinear VHE states and the formation of topological quasi-solitons. We have shown theoretically that it is crucial to have the type-II Dirac dispersion and a DW between two lattices of opposite Berry curvatures in order to achieve self-

trapping of the VHE solitons in the TRS-preserving topological systems. We would like to note that the nonlinear experiments with topological VHE states may also be implemented in femtosecond laser writing photonic lattices,[74] now that optical nonlinearity has been demonstrated in such a platform.[22,32,75] We believe that our results may prove relevant to other type-II systems such as nonlinear effects and high-frequency rectification in type-II topological semimetals[76] and may also enlighten new ideas in nonlinear non-Hermitian topological systems.[77] Moreover, there is still a plethora of interesting topics yet to be explored in nonlinear systems that could involve type-II Dirac points, including higher-order topological phases,[73,75,78] new physics arising from engineered longitudinal modulation,[79,80] synthetic dimensions,[81] and even the innovation of topological semiconductor laser technologies.[17–20] Thus, our work on nonlinear VHE states in engineered type-II lattices will surely stimulate further interest in topological photonics–an area that will continue to grow in the next decade.[82]

Acknowledgements

This work was supported by the National Key R&D Program of China (No. 2017YFA0303800), the National Natural Science Foundation of China (Nos. 12074308, 11922408, 11674180, and U1537210), and the Fundamental Research Funds for the Central Universities (Nos. xzy012019038 and 63213041). The authors appreciated Prof. Yaroslav V. Kartashov for helpful discussions on the robustness of quasi-solitons.

References

1. M. Z. Hasan and C. L. Kane, "Colloquium: topological insulators," *Rev. Mod. Phys.* **82**(4), 3045–3067 (2010)
2. X. L. Qi and S. C. Zhang, "Topological insulators and superconductor," *Rev. Mod. Phys.* **83**(4), 1057–1110 (2011).
3. F. D. M. Haldane and S. Raghu "Possible realization of directional optical waveguides in photonic crystals with broken time-reversal symmetry," *Phys. Rev. Lett.* **100**(1), 013904 (2008).
4. Z. Wang, Y. Chong, J. D. Joannopoulos, and M. Soljačić, "Observation of unidirectional backscattering-immune topological electromagnetic states," *Nature* **461**(7265), 772–775 (2009).
5. M. C. Rechtsman et al., "Photonic Floquet topological insulators," *Nature* **496**(7444), 196–200 (2013).
6. M. Hafezi et al., "Imaging topological edge states in silicon photonics," *Nat. Photonics* **7**(12), 1001–1005 (2013).
7. A. B. Khanikaev et al., "Photonic topological insulators," *Nat. Mater.* **12**(3), 233–239 (2013).
8. W. J. Chen et al., "Experimental realization of photonic topological insulator in a uniaxial metacrystal waveguide," *Nat. Commun.* **5**(1), 5782 (2014).
9. S. Stützer et al., "Photonic topological Anderson insulators," *Nature* **560**(7719), 461–465 (2018).
10. Y. Yang et al., "Realization of a three-dimensional photonic topological insulator," *Nature* **565**(7741), 622–626 (2019).
11. E. Lustig et al., "Photonic topological insulator in synthetic dimensions," *Nature* **567**(7748), 356–360 (2019).
12. S. Klembt et al., "Exciton-polariton topological insulator," *Nature* **562**(7728), 552–556 (2018).
13. Z. Yang et al., "Photonic Floquet topological insulators in a fractal lattice," *Light Sci. Appl.* **9**(1), 128 (2020).
14. L. Lu, J. D. Joannopoulos, and M. Soljacic, "Topological photonics," *Nat. Photonics* **8**(11), 821–829 (2014).
15. T. Ozawa et al., "Topological photonics," *Rev. Mod. Phys.* **91**(1), 015006 (2019).
16. D. Smirnova et al., "Nonlinear topological photonics," *Appl. Phys. Rev.* **7**(2), 021306 (2020).
17. A. Dikopoltsev et al., "Topological insulator vertical-cavity laser array," *Science* **373**(6562), 1514–1517 (2021).
18. G. Harari et al., "Topological insulator laser: theory," *Science* **359**(6381), eaar4003 (2018).
19. M. A. Bandres et al., "Topological insulator laser: experiments," *Science* **359**(6381), eaar4005 (2018).
20. Z. Yang et al., "Mode-locked topological insulator laser utilizing synthetic dimensions," *Phys. Rev. X* **10**(1), 011059 (2020).
21. Y. V. Kartashov and D. V. Skryabin, "Two-dimensional topological polariton laser," *Phys. Rev. Lett.* **122**(8), 083902 (2019).
22. L. J. M. Maczewsky et al., "Nonlinearity-induced photonic topological insulator," *Science* **370**(6517), 701–704 (2020).
23. Y. Hadad, A. B. Khanikaev, and A. Alù, "Self-induced topological transitions and edge states supported by nonlinear staggered potentials," *Phys. Rev. B* **93**(15), 155112 (2016).
24. Y. Lumer et al., "Self-localized states in photonic topological insulators," *Phys. Rev. Lett.* **111**(24), 243905 (2013).
25. M. J. Ablowitz, C. W. Curtis, and Y. P. Ma, "Linear and nonlinear traveling edge waves in optical honeycomb lattices," *Phys. Rev. A* **90**(2), 023813 (2014).
26. D. Leykam and Y. D. Chong, "Edge solitons in nonlinear-photonic topological insulators," *Phys. Rev. Lett.* **117**(14), 143901 (2016).
27. Y. V. Kartashov and D. V. Skryabin, "Modulational instability and solitary waves in polariton topological insulators," *Optica* **3**(11), 1228–1236 (2016).
28. D. R. Gulevich et al., "Exploring nonlinear topological states of matter with exciton-polaritons: edge solitons in Kagome lattice," *Sci. Rep.* **7**(1), 1780 (2017).
29. C. Liet et al., "Lieb polariton topological insulators," *Phys. Rev. B* **97**(8), 081103 (2018).
30. Y. Q. Zhang, Y. V. Kartashov, and A. Ferrando, "Interface states in polariton topological insulators," *Phys. Rev. A* **99**(5), 053836 (2019).
31. W. Zhang et al., "Coupling of edge states and topological Bragg solitons," *Phys. Rev. Lett.* **123**(25), 254103 (2019).
32. S. Mukherjee and M. C. Rechtsman, "Observation of Floquet solitons in a topological bandgap," *Science* **368**(6493), 856–859 (2020).
33. L. J. Maczewsky et al., "Observation of photonic anomalous Floquet topological insulators," *Nat. Commun.* **8**(1), 13756 (2017).
34. S. Mukherjee et al. "Experimental observation of anomalous topological edge modes in a slowly driven photonic lattice," *Nat. Commun.* **8**(1), 13918 (2017).
35. L. H. Wu and X. Hu, "Scheme for achieving a topological photonic crystal by using dielectric material," *Phys. Rev. Lett.* **114**(22), 223901 (2015).
36. K. F. Mak et al., "The valley Hall effect in MoS_2 transistors," *Science* **344**(6191), 1489–1492 (2014).
37. J.-W. Dong et al., "Valley photonic crystals for control of spin and topology," *Nat. Mater.* **16**(3), 298–302 (2017).
38. X. Wu et al. "Direct observation of valley-polarized topological edge states in designer surface plasmon crystals," *Nat. Commun.* **8**(1), 1304 (2017).
39. J. Noh et al., "Observation of photonic topological valley Hall edge states," *Phys. Rev. Lett.* **120**(6), 063902 (2018).
40. J.-W. Liu et al., "Valley photonic crystals," *Adv. Phys. X* **6**(1), 1905546 (2021).
41. Y. Zeng et al. "Electrically pumped topological laser with valley edge modes," *Nature* **578**(7794), 246–250 (2020).
42. Y. Yang et al. "Terahertz topological photonics for on-chip communication," *Nat. Photonics* **14**(7), 446–451 (2020).
43. M. I. Shalaev et al., "Robust topologically protected transport in photonic crystals at telecommunication wavelengths," *Nat. Nanotechnol.* **14**(1), 31–34 (2019).
44. D. A. Smirnova et al., "Topological edge states and gap solitons in the nonlinear Dirac model," *Laser Photonics Rev.* **13**(12), 1900223 (2019).

45. S. Suntsov et al., "Observation of discrete surface solitons," *Phys. Rev. Lett.* **96**(6), 063901 (2006).
46. K. G. Makris et al., "Discrete surface solitons," *Opt. Lett.* **30**(18), 2466–2468 (2005).
47. X. Wang et al., "Observation of two-dimensional surface solitons," *Phys. Rev. Lett.* **98**(12), 123903 (2007).
48. A. Szameit et al., "Observation of two-dimensional surface solitons in asymmetric waveguide arrays," *Phys. Rev. Lett.* **98**(17), 173903 (2007).
49. F. Lederer et al., "Discrete solitons in optics," *Phys. Rep.* **463**(1-3), 1–126 (2008).
50. Y. V. Kartashov, V. A. Vysloukh, and L. Torner, "Soliton shape and mobility control in optical lattices," *Prog. Opt.* **52**, 63–148 (2009).
51. J. Fleischer et al., "Observation of two-dimensional discrete solitons in optically induced nonlinear photonic lattices," *Nature* **422**(6928), 147–150 (2003).
52. L. Zeng and J. Zeng, "Gap-type dark localized modes in a Bose–Einstein condensate with optical lattices," *Adv. Photonics* **1**(4), 046004 (2019).
53. A. A. Soluyanov et al., "Type-II Weyl semimetals," *Nature* **527**(7579), 495–498 (2015).
54. G. G. Pyrialakos et al., "Emergence of type-II Dirac points in graphynelike photonic lattices," *Phys. Rev. Lett.* **119**(11), 113901 (2017).
55. B. Yang et al. "Ideal Weyl points and helicoid surface states in artificial photonic crystal structures," *Science* **359**(6379), 1013–1016 (2018).
56. J. Noh et al. "Experimental observation of optical Weyl points and Fermi arc-like surface states," *Nat. Phys.* **13**(6), 611–617 (2017).
57. G. G. Pyrialakos et al. "Symmetry-controlled edge states in the type-II phase of Dirac photonic lattices," *Nat. Commun.* **11**(1), 2074 (2020).
58. C. Hu et al. "Type-II Dirac photons at metasurfaces," *Phys. Rev. Lett.* **121**(2), 024301 (2018).
59. C. R. Mann et al., "Manipulating type-I and type-II Dirac polaritons in cavity-embedded honeycomb metasurfaces," *Nat. Commun.* **9**(1), 2194 (2018).
60. L. Xia et al., "Stretchable photonic Fermi arcs in twisted magnetized plasma," *Laser Photonics Rev.* **12**(1), 1700226 (2018).
61. M. Milićević et al., "Type-III and tilted Dirac cones emerging from flat bands in photonic orbital graphene," *Phys. Rev. X* **9**(3), 031010 (2019).
62. B. Yang et al., "Direct observation of topological surface-state arcs in photonic metamaterials," *Nat. Commun.* **8**(1), 97 (2017).
63. F. Li et al., "Weyl points and Fermi arcs in a chiral phononic crystal," *Nat. Phys.* **14**(1), 30–34 (2018).
64. X. Wu et al., "Deterministic scheme for two-dimensional type-II Dirac points and experimental realization in acoustics," *Phys. Rev. Lett.* **124**(7), 075501 (2020).
65. S. Xia et al., "Nontrivial coupling of light into a defect: the interplay of nonlinearity and topology," *Light Sci. Appl.* **9**(1), 147 (2020).
66. D. N. Christodoulides and M. I. Carvalho, "Bright, dark, and gray spatial soliton states in photorefractive media," *J. Opt. Soc. Am. B* **12**(9), 1628–1633 (1995).
67. K. C. Jin et al. "Parametric type-II Dirac photonic lattices," *Adv. Quantum Technol.* **3**(7), 2000015 (2020).
68. S. Mansha and Y. Chong, "Robust edge states in amorphous gyromagnetic photonic lattices," *Phys. Rev. B* **96**(12), 121405 (2017).
69. C. Liu et al., "Disorder-induced topological state transition in photonic metamaterials," *Phys. Rev. Lett.* **119**(18), 183901 (2017).
70. P. Zhou et al., "Photonic amorphous topological insulator," *Light Sci. Appl.* **9**, 133 (2019).
71. S. Xia et al. "Unconventional flatband line states in photonic Lieb lattices," *Phys. Rev. Lett.* **121**(26), 263902 (2018).
72. S. Xia et al., "Topological phenomena demonstrated in photorefractive photonic lattices," *Opt. Mater. Express* **11**(4), 1292–1312 (2021).
73. Z. Hu et al. "Nonlinear control of photonic higher-order topological bound states in the continuum," *Light Sci. Appl.* **10**(1), 164 (2021).
74. D. Tan et al., "Photonic circuits written by femtosecond laser in glass: improved fabrication and recent progress in photonic devices," *Adv. Photonics* **3**(2), 024002 (2021).
75. M. S. Kirsch et al., "Nonlinear second-order photonic topological insulators," *Nat. Phys.* **17**(9), 995–1000 (2021)
76. L. Zhang et al., "High-frequency rectifiers based on type-II Dirac fermions," *Nat. Commun.* **12**(1), 1584 (2021).
77. S. Xia et al., "Nonlinear tuning of PT symmetry and non-Hermitian topological states," *Science* **372**(6537), 72–76 (2021).
78. B. Xie et al., "Higher-order band topology," *Nat. Rev. Phys.* **3**(7), 520–532 (2021).
79. W. Song et al., "Subwavelength self-imaging in cascaded waveguide arrays," *Adv. Photonics* **2**(3), 036001 (2020).
80. K. C. Jin et al., "Rabi oscillations of Azimuthons in weakly nonlinear waveguides," *Adv. Photonics* **2**(4), 046002 (2020).
81. K. Wang et al., "Multidimensional synthetic chiral-tube lattices via nonlinear frequency conversion," *Light Sci. Appl.* **9**(1), 132 (2020).
82. Z. Chen and M. Segev, "Highlighting photonics: looking into the next decade," *eLight* **1**, 2 (2021).

Hua Zhong received her BS degree from Qingdao University of Technology in 2015 and her master's degree from Xi'an Jiaotong University in 2018. Currently, she is pursuing her PhD as a student under the supervision of Dr. Yiqi Zhang at the School of Electronic Science and Engineering of Xi'an Jiaotong University. Her focus is topological and waveguide array physics.

Shiqi Xia received his PhD from Nankai University, Tianjin, China, in 2021. He is currently a postdoc fellow at the School of Physics of Nankai University. His research interests include nonlinear optics, topological photonics, non-Hermitian system, as well as synthetic dimensions.

Yiqi Zhang received his PhD from Xi'an Institute of Optics and Precision Mechanics, Chinese Academy of Sciences, Xi'an, China, in 2011. He is currently an associate professor at the School of Electronic Science and Engineering of Xi'an Jiaotong University. His current research interests include topological photonics and quantum-optical analogies.

Yongdong Li received his PhD from Xi'an Jiaotong University, Xi'an, China, in 2005. He is currently a professor at the School of Electronic Science and Engineering of Xi'an Jiaotong University. His research interests include modeling and applications of plasmas.

Daohong Song received his PhD from Nankai University, Tianjin, China, in 2009. He is currently a professor at the TEDA Applied Physics Institute and School of Physics of Nankai University. His current research interests include topological photonics and nonlinear optics.

Chunliang Liu received his BS and MS degrees from Xi'an Jiaotong University, Xi'an, China, in 1982 and 1987, respectively, and his PhD from the China Institute of Atomic Energy, Beijing, China, in 1992. He is currently a professor at the School of Electronic Science and Engineering of Xi'an Jiaotong University. He actively conducts research in flat panel displays, plasma discharge physics, and high-power microwave technology.

Zhigang Chen earned his PhD from Bryn Mawr College in 1995. After two years of postdoctoral research, he was promoted to the rank of Senior Research Staff Member at Princeton University before joining the faculty at San Francisco State University in 1998. He is currently a specially appointed chair professor at Nankai University. His research interests include nonlinear optics, topological photonics, and optical manipulation. He is a fellow of OSA and APS.